^{170}Yb Mössbauer and neutron diffraction measurements on spin-chain Yb_2BaNiO_5

2000 J. Phys.: Condens. Matter 12 9973

(http://iopscience.iop.org/0953-8984/12/48/313)

J. Phys.: Condens. Matter **12** (2000) 9973–9983. Printed in the UK PII: S0953-8984(00)15465-7

^{170}Yb Mössbauer and neutron diffraction measurements on spin-chain Yb_2BaNiO_5

J A Hodges†, P Bonville†, N Genand-Riondet†, K Tomala‡, N Kernavanois§, E Ressouche§, J P Sanchez§ and P Vulliet§

† CEA-Saclay, DRECAM/SPEC, 91191 Gif sur Yvette, France
‡ M Smoluchowski Institute of Physics, Jagellonian University, Cracow, Poland
§ CEA-Grenoble, DRFMC/SPSMS, 38054 Grenoble Cédex 9, France

Received 13 July 2000, in final form 13 October 2000

Abstract. The Ni ($S = 1$) chain compound Yb_2BaNiO_5 (space group: *Immm*) is the end magnetic member of the isomorphous rare earth series. We have studied its magnetic properties using ^{170}Yb Mössbauer spectroscopy and neutron diffraction. Magnetic order is induced into the Ni^{2+} chains through the polarization of the Yb^{3+} and leads to an ordering temperature of 8.8 K. The Ni^{2+} moments, saturated value 1.1 μ_B, are antiferromagnetically aligned close to the *c*-axis and the Yb^{3+} moments, saturated value 0.6 μ_B, are antiferromagnetically aligned at an angle of 55° to the *c*-axis and close to the (*ac*) plane. The thermal evolution of the Yb^{3+} moment is well described with a phenomenological molecular-field model. The value derived for the effective polarizing field acting on the Ni^{2+} when expressed per Yb^{3+} moment is much higher than the equivalent value for any of the other rare earths.

1. Introduction

In Y_2BaNiO_5, the Ni^{2+} ions form an arrangement of well separated parallel chains [1, 2]. Strong intra-chain magnetic interactions lift the degeneracy of the single-ion spin–orbit-derived $S = 1$ ground state to leave a (non-magnetic) singlet ground level with a gap of approximately 100 K to the lowest excited state [3, 4]. The Ni^{2+} thus behave in line with the Haldane scenario for uncoupled antiferromagnetic Heisenberg $S = 1$ chains. It has previously been reported that the Y^{3+} may be replaced by most of the rare earths without modifying the crystal structure [2]. The magnetic rare-earth ions then introduce a coupling between the chains and Ni^{2+} magnetic ordering appears at low temperatures. Magnetic ordering also appears within the rare-earth sublattice [5–8] and, in fact, the Ni and rare-earth sublattices share a common ordering temperature. The magnetic polarization of the Ni^{2+} which is triggered by the rare earth does not lead to the suppression of the gap, which is instead renormalized in the magnetically ordered region [9].

The magnetic behaviour of the R_2BaNiO_5 has been previously examined for compounds having R^{3+} from Pr^{3+} to Tm^{3+} [5–15]. We report here what appears to be the first study of the magnetic properties for $R^{3+} = Yb^{3+}$. Our results, obtained from a ^{170}Yb Mössbauer spectroscopy and neutron diffraction study, concern the size and direction of the Ni^{2+} and Yb^{3+} magnetic moments and the size of the intersublattice effective exchange fields. Yb_2BaNiO_5 shows the particularity of a relatively small saturated rare-earth moment (0.6 μ_B) (well canted away from the crystal *c*-axis and from the (*ab*) basal plane), a relatively low common R^{3+} and Ni^{2+} ordering temperature (8.8 K), but a relatively important low-temperature saturated

0953-8984/00/489973+11$30.00

induced Ni^{2+} moment of 1.1 μ_B (in the (bc) plane and slightly canted away from the c-axis). The effective exchange polarization (the size of the induced Ni^{2+} moment divided by the size of the polarizing rare-earth moment) is much higher for Yb^{3+} than for the other rare earths.

2. Sample and magnetic susceptibility

The samples of Yb_2BaNiO_5 were prepared by combining Ni and Yb_2O_3 dissolved in concentrated nitric acid with an aqueous solution of $Ba(NO_3)_2$ and then heating the dried mixture to 1000 °C. This method gave more reproducible results than could be obtained by simply heating the constituent oxides in air. The room temperature x-ray measurements evidence the same structure type (Nd_2BaNiO_5; space group: $Immm$) as is shown by most of the other R_2BaNiO_5 [2]. (Yb_2BaNiO_5 with the Sm_2BaCuO_5 structure type (space group: $Pmma$) may be obtained by heating above 1100 °C.) In this structure (figure 1), compressed corner-sharing NiO_6 octahedra are aligned along the a-axis. The Ni–Ni nearest-neighbour distance along the chains is 0.38 nm and the smallest intra-chain Ni–Ni distance is 0.66 nm. Each Yb^{3+} has seven oxygen neighbours which form a capped trigonal prism.

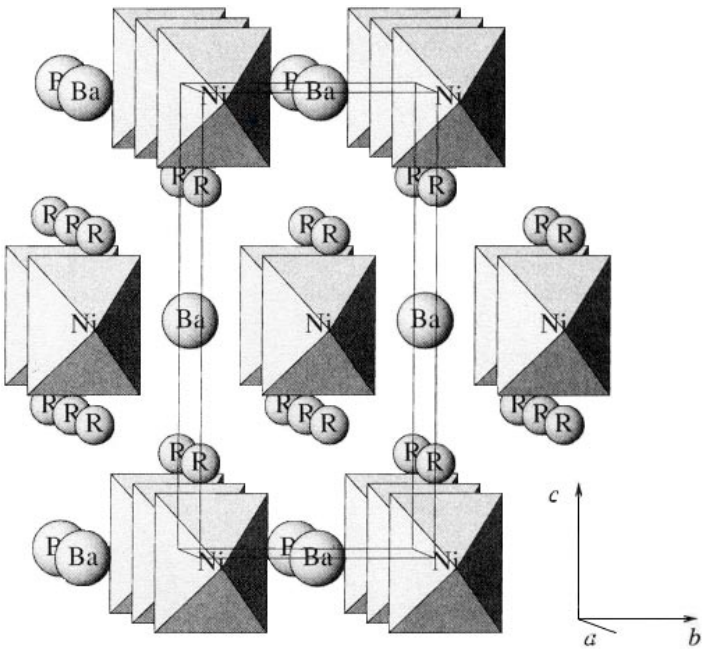

Figure 1. The crystal structure of the R_2BaNiO_5 (space group: $Immm$). The Ni–O chains are aligned along the a-axis. (Adapted from reference [15].)

The thermal dependence of the inverse susceptibility obtained in a field of 8 mT is shown in figure 2. The signal is dominated by the contribution coming from the Yb^{3+} ions and the curvature observed with increasing temperature is due to crystal-field effects. Because of the Yb^{3+} contribution, it is not possible to use the susceptibility data to obtain a value of the Ni spin gap as was done for Y_2BaNiO_5 [3]. The low-temperature behaviour is shown on an expanded scale in the inset of figure 2. One weak anomaly is visible near 9 K which, as is shown below, corresponds to the magnetic ordering temperature.

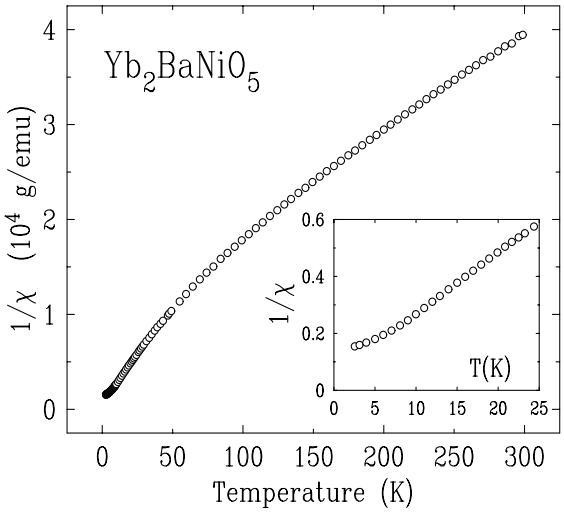

Figure 2. The inverse susceptibility for Yb_2BaNiO_5 in a field of 8 mT. The weak anomaly in the inset near 9 K corresponds to the onset of magnetic ordering.

3. ^{170}Yb Mössbauer absorption measurements

The ^{170}Yb Mössbauer absorption measurements were made over the temperature range 50 to 0.03 K using a source of neutron-irradiated TmB_{12} and a triangular velocity sweep. For ^{170}Yb, $I_g = 0$, $I_{ex} = 2$, $E_\gamma = 84$ keV, 1 mm s^{-1} = 68 MHz. Some results at selected temperatures are shown in figure 3.

The data were fitted in terms of the standard fast-relaxation magnetic-plus-quadrupole hyperfine Hamiltonian appropriate for the Yb^{3+} point symmetry with the coordinate axes $(\vec{x}, \vec{y}, \vec{z})$ defined relative to the principal axes of the electric field gradient:

$$\mathcal{H} = \frac{eQV_{zz}}{8}\left[I_z^2 - \frac{I(I+1)}{3} + \frac{\eta}{6}(I_+^2 + I_-^2)\right] - g_n\beta_n H(I_z\cos\theta + I_x\sin\theta\cos\phi + I_y\sin\theta\sin\phi). \quad (1)$$

The local z-axis is along the principal axis of the electric field gradient tensor and for the hyperfine field (H), the polar angle (θ) is relative to the z-axis and the azimuthal angle (ϕ), within the (xy) plane, is relative to the x-axis. Because the rare-earth site has two orthogonal mirror planes for symmetry elements, the $\vec{x}$-, $\vec{y}$- and $\vec{z}$-axes must each lie along one of the crystal axes ($\vec{a}$, $\vec{b}$, $\vec{c}$).

At 10 K (figure 3), there is no hyperfine field and a good line fit is obtained using only the quadrupole part of equation (1). We obtain $eQV_{zz} = (\Delta E_Q)_{zz} = 17.2 \pm 0.16$ mm s^{-1} and $\eta = 0.52 \pm 0.02$. The total electric field gradient is made up of two parts, the contribution coming from the non-spherical distribution of lattice charges and the self-ion contribution coming from the non-spherical 4f-shell distribution. As mentioned, the principal axes of the two tensors will lie along the crystal $\vec{a}$-, $\vec{b}$- and $\vec{c}$-axes but there is no reason for the principal components of each to be parallel. In fact, we find that the two principal components are not parallel. By comparing the ^{170}Yb Mössbauer and neutron diffraction data (section 5) we find that the total electric field gradient has its principal axis along a crystal $\vec{a}$-direction and its components are $(\Delta E_Q)_{aa} = 17.2$, $(\Delta E_Q)_{bb} = -4.1$ and $(\Delta E_Q)_{cc} = -13.1$ mm s^{-1}. The electric field gradient associated with the lattice charges may be estimated by scaling the values

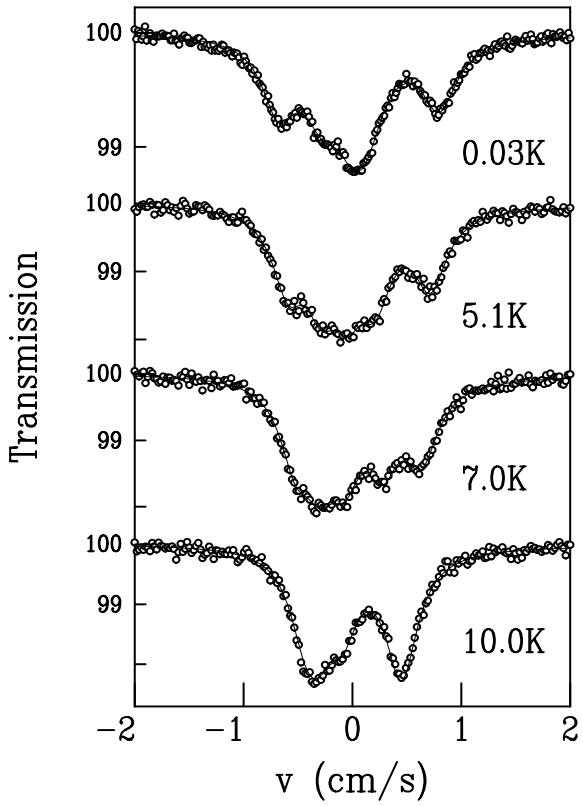

Figure 3. $^{170}Yb^{3+}$ Mössbauer spectra for Yb_2BaNiO_5. A quadrupole lineshape is seen at 10 K in the paramagnetic region and an additional hyperfine field is visible at temperatures below the magnetic ordering temperature of 8.8 K.

obtained from ^{155}Gd Mössbauer measurements on the S-state ion Gd^{3+} in Gd_2BaNiO_5 [16]. It has its principal direction along the $\vec{c}$-direction and the values are $(\Delta E_Q^{latt})_{cc} = 10.0$, $(\Delta E_Q^{latt})_{bb} = -3.2$ and $(\Delta E_Q^{latt})_{aa} = -6.8$ mm s^{-1}. Subtracting the lattice contribution from the total contribution leads to the 4f-shell components $(\Delta E_Q^{4f})_{aa} = 24.0$, $(\Delta E_Q^{4f})_{bb} = -0.9$ and $(\Delta E_Q^{4f})_{cc} = -23.1$ mm s^{-1}. The 4f contribution thus has its principal axis along the $\vec{a}$-direction.

The examination of the thermal dependence of the quadrupole interaction provides some information concerning the energies of the crystal-field levels. The crystal electric field splits the Yb^{3+} $^2F_{7/2}$ level into four Kramers doublets each with a different associated 4f-shell electric field gradient. As the temperature is increased, the total gradient, which, together with the lattice charge contribution, involves the Boltzmann average of the gradient for the four Kramers doublets, will thus begin to depend on temperature when the first excited crystal-field level is significantly populated. Experimentally, we observe that at 50 K the quadrupole interaction remains the same as at 10 K and at 100 K it shows only a very small decrease of 3%. This suggests that the energy of the first excited crystal-field doublet is of the order of 100 K. That is, it is relatively well separated from the ground-state doublet. The relatively large crystal-field splitting means that in the temperature range where magnetic ordering takes place, only the ground Kramers doublet is populated.

A hyperfine field becomes visible in the Mössbauer lineshape when the temperature is lowered below about 9 K (figure 3) and the field reaches a saturated low-temperature value of 60 T. For the data from 0.03 to 4.2 K, we find that when the two quadrupole parameters ($(\Delta E_Q)_{zz}$ and η) and the three magnetic hyperfine parameters (H, θ and ϕ) of equation (1) are all fitted, the values of $(\Delta E_Q)_{zz}$ and η remain essentially the same as in the paramagnetic region at 10 K. The appearance of the molecular field which acts on the Yb^{3+} does not change the electric field gradient—showing that the field does not lead to any mixing of the wave functions of the ground-state Kramers doublet with those of the excited Kramers doublets. This again indicates that the first excited crystal-field level is well separated from the ground state. For the hyperfine-field fits between 4.2 K and the ordering temperature (8.8 K), we imposed the quadrupole parameters at their common high-temperature (10 K) and low-temperature (0.03 to 4.2 K) values.

For Yb^{3+}, J is a good quantum number, so the 4f-shell magnetic moment is proportional to the hyperfine field†. The saturated value of the hyperfine field (60 T) corresponds to a saturated Yb^{3+} moment of 0.6 μ_B. The thermal dependence of the Yb^{3+} magnetic moment obtained from that of the hyperfine field is given in figure 4. The direction of the field relative to the principal axes of the electric field gradient is independent of temperature and corresponds to the values $\theta = 39^\circ \pm 3^\circ$, $\phi = 65^\circ \pm 5^\circ$. We discuss the direction of the Yb^{3+} magnetic moment relative to the crystal axes in section 5 and the thermal dependence of the moments in section 6.

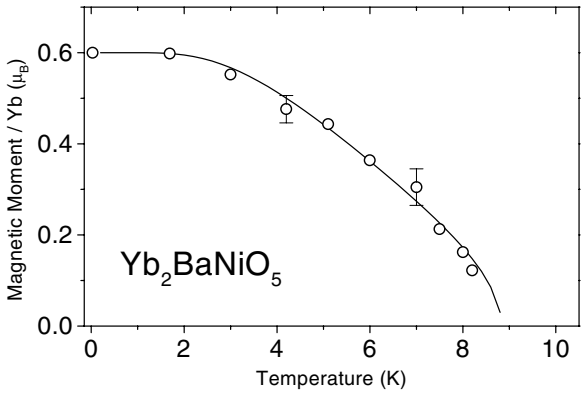

Figure 4. The thermal dependence of the Yb^{3+} magnetic moment in Yb_2BaNiO_5 as obtained from ^{170}Yb Mössbauer measurements. The solid line was calculated using the phenomenological two-sublattice model described in the text.

4. Neutron diffraction measurements

The neutron diffraction measurements were carried out at the high-flux reactor of the Institut Laue–Langevin at Grenoble on the D1B diffractometer ($\lambda = 2.524$ Å, $2\theta_{min} = 11.9^\circ$). The measurements were made at two temperatures, 15 K in the paramagnetic state and 2 K in the essentially saturated magnetic state. The powder diffraction pattern analysis was made by Rietveld profile refinement using the software FULLPROF [17]. The scattering lengths were taken from reference [18] and the Yb and Ni form factors from reference [19].

† We use the relation $M\ (\mu_B) = 0.01H$ (T) to derive the Yb^{3+} magnetic moment from the measured hyperfine field.

At 15 K, the pattern evidences the same crystal structure type (Nd_2BaNiO_5) as shown by the room temperature x-ray analysis and the lattice parameters are $a = 3.7568(9)$, $b = 5.715(2)$ and $c = 11.213(3)$ Å. Small amounts (<2%) of the impurities Yb_2BaNiO_5 with the Sm_2BaNiO_5 structure and Yb_2O_3 were detected, but their presence has no detrimental influence on the analysis. At 2 K, the magnetic Bragg peaks can be indexed with a propagation vector $(1/2, 0, 1/2)$ as is the case for the other R_2BaNiO_5. The magnetic contribution was isolated by subtracting the purely nuclear signal seen at 15 K from the total signal seen at 2 K (figure 5). The adjustable parameters in the refinement were the components of the Yb^{3+} and Ni^{2+} moments along each of the crystallographic axes and the values obtained are given in table 1. Figure 6 presents a schematic representation of the directions of the Ni^{2+} and Yb^{3+} moments.

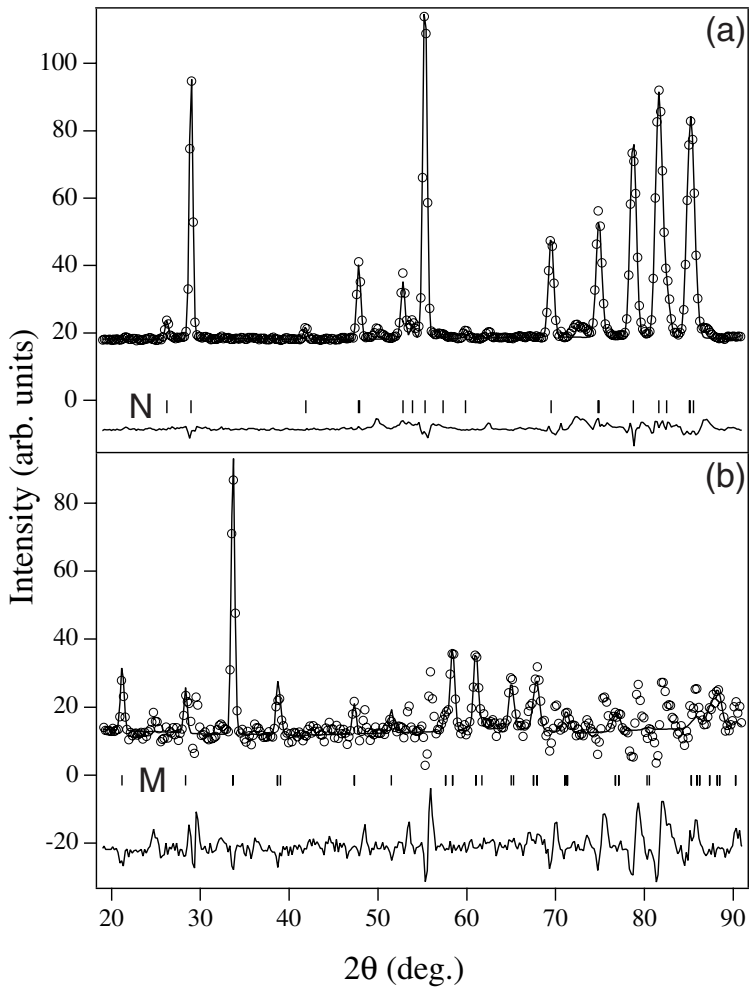

Figure 5. Measured (symbols) and calculated (solid line) powder diffraction patterns for Yb_2BaNiO_5. (a) The diffraction pattern in the paramagnetic state at 15 K. (b) The magnetic difference pattern $I(2\text{ K}) - I(15\text{ K})$. The ticks indicate the Bragg reflections: N: nuclear; M: magnetic. The lower curve below each pattern represents the difference between the observed pattern and the Rietveld refinement.

Table 1. From neutron diffraction measurements on Yb_2BaNiO_5 at 2 K: components of the Yb^{3+} and Ni^{2+} magnetic moments along the three crystal axes (M_a, M_b and M_c) together with the size of the total moment (M).

	M_a (μ_B)	M_b (μ_B)	M_c (μ_B)	M (μ_B)
Yb	−0.403(2)	0.083(58)	0.270(12)	0.49(4)
Ni	−0.036(7)	0.182(104)	1.057(18)	1.07(7)

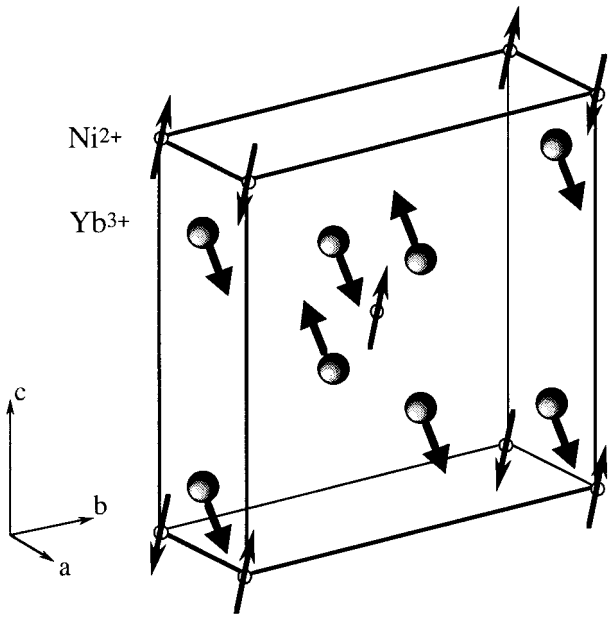

Figure 6. A schematic representation of the directions of the Ni^{2+} and Yb^{3+} moments in Yb_2BaNiO_5. A single unit cell is shown and for clarity only the Ni and Yb atoms are included. The Ni^{2+} moments are aligned close to the c-axis and the Yb^{3+} moments are canted by 53° from the c-axis and by 13° from the (ac) plane (see table 1).

5. Directions of the Yb^{3+} moments and of the ^{170}Yb electric field gradient

The neutron measurements provide the directions of the Yb^{3+} moment relative to the crystal axes ($\vec{a}$, $\vec{b}$, $\vec{c}$). The Mössbauer measurements provide the directions of the Yb^{3+} moment relative to the coordinate frame of the electric field gradient ($\vec{x}$, $\vec{y}$, $\vec{z}$). (We recall that by symmetry, each principal axis of the electric field gradient must lie along a crystal axis.) By combining the two sets of results, we can establish the directions of the principal axes of the electric field gradient relative to the crystal axes.

Figure 7 defines the two coordinate frames. The neutron measurements provide the information that the Yb^{3+} moment makes an angle of $\theta_a = 35^\circ \pm 7^\circ$ with the $\vec{a}$-axis, $\theta_b = 80^\circ \pm 8^\circ$ with the $\vec{b}$-axis and $\theta_c = 57^\circ \pm 5^\circ$ with the $\vec{c}$-axis. The Mössbauer measurements provide the information that the moment makes an angle of $\theta_z = 39^\circ \pm 3^\circ$ with the principal axis of the electric field gradient. The comparison of the two sets of data shows that the principal axis of the electric field gradient ($\vec{z}$) must lie along the $\vec{a}$-axis. This choice is reinforced by the coherence which also exists between the two values obtained for the azimuthal angle (ϕ). The Mössbauer measurement directly provides the value $65^\circ \pm 5^\circ$ and

the neutron measurements of M_a, M_b and M_c provide the value $\phi = 73^\circ \pm 15^\circ$. The values found for the different angles defined in figure 7 are given in table 2. The Mössbauer and the neutron measurements thus lead to a coherent solution for the direction of the Yb^{3+} magnetic moments which are found to lie at an angle of $55^\circ \pm 4^\circ$ to the $\vec{c}$-axis and $13^\circ \pm 3^\circ$ from the (ac) plane. These angles are independent of temperature. Although the two techniques lead to coherent results for the directions of the moments, they provide two slightly different values for the absolute size. One way to explain this difference is to first note that the Mössbauer measurements provide the total size of each individual moment whereas the neutron measurements provide the size of the correlated moments and then to assume that a small proportion of the moments are not detected by the neutron measurements because they are not directionally correlated.

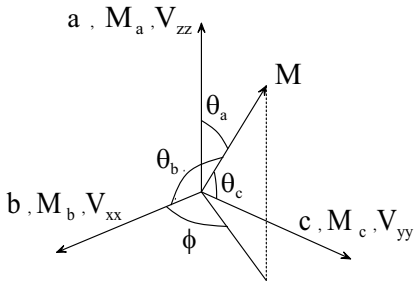

Figure 7. Coordinate frames appropriate for Yb_2BaNiO_5. a, b and c refer to the crystal axes and x, y and z to the axes of the electric field gradient. The values for the various angles that define the direction of the Yb^{3+} magnetic moment (M) are given in table 2.

Table 2. From ^{170}Yb Mössbauer and neutron diffraction measurements on Yb_2BaNiO_5: total sizes (M) and directions (θ_a, θ_b and θ_c) relative to the crystal axes (a, b and c) of the saturated low-temperature Yb^{3+} moment. ϕ represents the moment direction in the (bc) plane measured from the b-axis (see figure 7). The values without square brackets are directly measured and those within square brackets are derived.

	M (μ_B)	θ_a (deg)	θ_b (deg)	θ_c (deg)	ϕ (deg)
^{170}Yb	0.60(3)	39(3)	[75(4)]	[55(4)]	65(5)
Neutrons	0.49(4)	35(7)	80(8)	57(5)	[73(15)]

6. Thermal dependence of the Yb^{3+} moments

Although the magnetic ordering temperature of the Yb^{3+} is relatively low (8.8 K), it is much higher than that observed for any known compound which contains only Yb^{3+} as the magnetic ions. It is thus already clear that the Yb^{3+} are polarized by fields coming from the Ni^{2+} sublattice, meaning that the Ni^{2+} sublattice must also carry magnetic moments. The presence of the Yb^{3+} leads to a polarization of the Ni^{2+} and to a magnetic coupling between the chains in a similar manner to that observed for the other R_2BaNiO_5. The behaviour of this ordering induced into a coupled-chain system differs from that occurring in 'conventional' magnetic systems. For example, even at $T = 0$, the individual Ni moments may not be saturated and they may still depend on the size of the local magnetizing field. Further, when the temperature is less than the spin-gap value, the size of the Ni moment may still depend on the size of the local magnetizing field but it may be largely independent of temperature (in as much as the field is independent of temperature).

The initial description of the interrelation between the Ni^{2+} and R^{3+} moments using a molecular-field treatment was given by García-Munoz and co-workers [8] who used an

empirical function to fit the observed thermal dependence of the Ni^{2+} moment and then injected this into the molecular-field expressions. Yokoo *et al* [12] instead made use of the experimental observation that in Nd_2BaNiO_5 the size of the Ni^{2+} moment is a non-linear function of the size of the Nd^{3+} moments (that is, of the field produced by the Nd^{3+} moment) with a tendency towards saturation and that the sizes of the two moments could be described by an empirical relation. For the case of Ni^{2+} moments (M^{Ni}) and the Yb^{3+} moments (M^{Yb}) the equivalent empirical relation is written as follows:

$$M^{Ni} = A \tan^{-1}(BM^{Yb}) \tag{2}$$

where the constants A and B are to be found from comparison with the experimental data. The Ni^{2+}–Ni^{2+} interaction is not included explicitly as a separate term because its role in the magnetization process is already implicitly included through the use of the chosen empirical relation.

The thermal dependence of M^{Yb} is taken to follow the standard Brillouin function dependence for $S' = 1/2$:

$$M_T^{Yb} = M_0^{Yb} B_{1/2}\left[\frac{M_0^{Yb} H^{Yb}}{k_B T}\right]. \tag{3}$$

As there is no evidence of any contribution to the field arising from within the Yb^{3+} sublattice (there is no evidence of any low-temperature anomaly which could be linked to a measurable Yb^{3+}–Yb^{3+} interaction), we consider that the field acting on the Yb^{3+} is produced only by the Ni^{2+} sublattice and it is written as follows:

$$H^{Yb} = \alpha M^{Ni}. \tag{4}$$

From these equations we obtain

$$M_T^{Yb} = M_0^{Yb} B_{1/2}\left[\frac{M_0^{Yb}\alpha A \tan^{-1}(BM_T^{Yb})}{k_B T}\right]. \tag{5}$$

The solid line in figure 4, which provides a good description of the thermal dependence of M_T^{Yb}, was obtained from equation (5) using $M_0^{Yb} = 0.6\ \mu_B$, $A = 1.07\ \mu_B$, $B = 2.88\ \mu_B^{-1}$ and $\alpha = 13.0\ \mathrm{T}\ \mu_B^{-1}$. Equivalently good fits could be obtained with A up to 1.3 but the value 1.07 is preferred because it leads to a calculated limiting low-temperature value for M^{Ni} which agrees with the 2 K neutron measurement (1.1 μ_B). The empirical relation given as equation (2) thus provides a good description of the experimental interdependence of M^R and M^{Ni} for the case $R^{3+} = Yb^{3+}$, as it does for $R^{3+} = Nd^{3+}$ [12], Er^{3+} [13] and Dy^{3+} [16]. As there are twice as many Yb^{3+} as Ni^{2+}, the effective field acting on a Ni^{2+} ion due to the effective coupling with the Yb^{3+} is given by

$$H^{Ni} = 2\alpha M^{Yb}. \tag{6}$$

The parameter 2α is thus a measure of the relative strength of the effective field acting on the Ni^{2+} per unit of rare-earth moment. In the present case, $2\alpha = 26.0\ \mathrm{T}\ \mu_B^{-1}$.

The values obtained for the different parameters for Yb_2BaNiO_5 are given in table 3 which also presents the equivalent values for the other R_2BaNiO_5 with the Kramers ions: Nd^{3+} [13], Dy^{3+} [16] and Er^{3+} [13, 16]. The values quoted from reference [13] are used in conjunction with the definition of equation (2).

These results together with the other elements of this study are considered in the next section.

Table 3. For four R_2BaNiO_5 with Kramers ion rare earths (R): T_{order} is the combined ordering temperature of the R^{3+} and Ni^{2+} sublattices with M_0^R and M_0^{Ni} the respective values for the saturated magnetic moments. The parameters A, B and 2α appear in the expressions given in the text.

R	T_{order} (K)	M_0^R (μ_B)	M_0^{Ni} (μ_B)	A (μ_B)	B (μ_B^{-1})	2α (T μ_B^{-1}(R))	Reference
Nd^{3+}	48	2.68	1.55	1.17	1.7	16.4	[13]
Dy^{3+}	65	7.9	1.53	1.27	0.32	5.66	[16]
Er^{3+}	33	7.9	1.54	1.17	0.43	3.66	[13, 16]
Yb^{3+}	8.8	0.6	1.07	1.07	2.88	26.0	This work

7. Summary and discussion

In the Ni ($S = 1$) spin-chain compound Yb_2BaNiO_5 (structure type Nd_2BaNiO_5; SG: $Immm$), we find that the Yb^{3+} ion has a well isolated $S' = 1/2$ ground state with anisotropic properties. By comparing the ^{170}Yb Mössbauer and neutron diffraction results, we find that the principal axis of the total electric field gradient on the Yb^{3+} is along the $\vec{a}$-axis. The lattice contribution to the gradient has its principal component along the $\vec{c}$-axis and the principal axis of the 4f-shell contribution to the gradient is along the $\vec{a}$-axis. Magnetic ordering occurs below 8.8 K and the Yb^{3+} magnetic moments are aligned along a temperature independent direction which is canted by 55° from the $\vec{c}$-axis and by 13° from the (ac) plane. The Yb^{3+} moments are thus not aligned along their self-ion easy-anisotropy direction. This suggests that the dominant polarizing field, coming from the Ni sublattice, must also be canted away from the principal crystallographic axis directions. The neutron diffraction measurements show, however, that the correlated Ni^{2+} ordered moments are aligned fairly closely with the $\vec{c}$-axis (perpendicular to the axis of the chains).

We examined the relation between the Ni^{2+} moment and the Yb^{3+} moment using the phenomenological model introduced to describe Nd_2BaNiO_5 [12] and which was also found to describe Er_2BaNiO_5 [13]. In this approach the size of the Ni moment is simply expressed as an empirical function of the size of the rare-earth moment and the rare-earth moment is described with a standard molecular-field expression. We find that this approach works well for Yb_2BaNiO_5. For each of the rare earths shown in table 3, the asymptotic value of M^{Ni} ($=1.57A$ from equation (2)) is in the neighbourhood of 2 which would be the value of the saturated moment associated with individual Ni^{2+} ions. Table 3 also shows that the magnetic ordering temperature varies considerably depending on the rare earth and in fact, they roughly scale with the value of the spin component of the rare earth ($(g_J - 1)J$). This suggests, as expected, that the exchange is spin based. The effective staggered field acting on the Ni when expressed per unit of the rare-earth moment (the parameter 2α in table 3) varies considerably for the different rare earths and it is highest for Yb_2BaNiO_5. The observed variation does not seem to fit into any coherent picture and in fact it is not at present clear how this phenomenological field is related to the actual field produced by the rare earth.

Finally we note that the phenomenological model for the staggered magnetization of the Ni chains implicitly assumes that the effective interaction between the rare-earth and Ni sublattices is of the Ising type [14]. In Yb_2BaNiO_5, however, the two sublattices are strongly canted. For the Ising case, the transverse excitations on the chains are decoupled from those on the rare-earth sublattice and the neutron scattering data show that it is the transverse gap that scales with the reduced staggered chain moment [14]. Our planned inelastic neutron scattering measurements on Yb_2BaNiO_5 will examine whether this continues to be the case when the sublattice moments are canted.

References

[1] Buttrey D J, Sullivan J D and Rheingold A L 1990 *J. Solid State Chem.* **88** 291
[2] García-Matres E, Martínez J L, Rodríguez-Carvajal J, Alonso J, Salinas-Sánchez A and Sáez-Puche R 1993 *J. Solid State Chem.* **103** 322
[3] Darriet J and Regnault L P 1993 *Solid State Commun.* **86** 409
[4] Shimizu T, Maclaughlin D E, Hammel P C, Thompson J D and Cheong S-W 1995 *Phys. Rev.* B **52** R9835
[5] Chepurko G G, Kazei Z A, Kudrjavtsev D A, Levitin R Z, Mill B V, Popova M N and Snegirev V V 1991 *Phys. Lett.* A **157** 81
[6] Sachan V, Buttrey D J, Tranquada J M and Shirane G 1994 *Phys. Rev.* B **49** 9658
[7] Alonso J A, Amador J, Martinez J L, Rasines I, Rodríguez-Carvajal J and Sáez-Puche R 1990 *Solid State Commun.* **76** 467
[8] García-Matres E, García-Munoz J L, Martinez J L and Rodríguez-Carvajal J 1995 *J. Magn. Magn. Mater.* **149** 363
[9] Zheludev A, Tranquada J M, Vogt T and Buttrey D J 1996 *Phys. Rev.* B **54** 7210
[10] Zheludev A, Hill J P and Buttrey D J 1996 *Phys. Rev.* B **54** 7216
[11] Yokoo T, Zheludev A, Nakamura M and Akimitsu J 1997 *Phys. Rev.* B **55** 11 516
[12] Yokoo T, Raymond S, Zheludev A, Maslov S, Ressouche E, Zaliznyak I, Erwin R, Nakamura M and Akimitsu J 1998 *Phys. Rev.* B **58** 14 424
[13] Zheludev A, Ressouche E, Maslov S, Yokoo T, Raymond S and Akimitsu J 1998 *Phys. Rev. Lett.* **80** 3630
[14] Maslov S and Zheludev A 1998 *Phys. Rev. Lett.* **80** 5786
[15] Stewart G A, Harker S J, Strecker M and Wortmann G 2000 *Phys. Rev.* B **61** 6220
[16] Vulliet P, Sanchez J P, Kernavanois N, Ressouche E, Tomala K, Hodges J A and Bonville P unpublished
[17] Rodríguez-Carvajal J 1993 *Physica* B **192** 55
[18] Koester L, Rauch H and Seymann E 1991 *At. Data Nucl. Data Tables* **49** 65
[19] Brown P J 1992 *International Tables for Crystallography* ed A J C Wilson (Dordrecht: Kluwer) pp 391–9